Structural Insight into the Zinc Finger CW Domain as a Histone Modification Reader

Fahu He,[1] Takashi Umehara,[1] Kohei Saito,[1] Takushi Harada,[1] Satoru Watanabe,[1] Takashi Yabuki,[1] Takanori Kigawa,[1,2] Mari Takahashi,[1] Kanako Kuwasako,[1] Kengo Tsuda,[1] Takayoshi Matsuda,[1] Masaaki Aoki,[1] Eiko Seki,[1] Naohiro Kobayashi,[1] Peter Güntert,[3,4] Shigeyuki Yokoyama,[1,5,*] and Yutaka Muto[1,*]

[1]RIKEN Systems and Structural Biology Center, 1-7-22 Suehiro-cho, Tsurumi-ku, Yokohama 230-0045, Japan
[2]Tokyo Institute of Technology, 4259 Nagatsuta-cho, Midori-ku, Yokohama 226-8502, Japan
[3]Tatsuo Miyazawa Memorial Program, RIKEN Genomic Sciences Center, Yokohama 230-0045, Japan
[4]Institute of Biophysical Chemistry, Center for Biomolecular Magnetic Resonance, and Frankfurt Institute of Advanced Studies, Goethe University Frankfurt, Max-von-Laue-Strasse 9, 60438 Frankfurt am Main, Germany
[5]Department of Biophysics and Biochemistry, Graduate School of Science, The University of Tokyo, 7-3-1 Hongo, Bunkyo-ku, Tokyo 113-0033, Japan
*Correspondence: yokoyama@biochem.s.u-tokyo.ac.jp (S.Y.), ymuto@gsc.riken.jp (Y.M.)
DOI 10.1016/j.str.2010.06.012

SUMMARY

The zinc finger CW (zf-CW) domain is a motif of about 60 residues that is frequently found in proteins involved in epigenetic regulation. Here, we determined the NMR solution structure of the zf-CW domain of the human zf-CW and PWWP domain containing protein 1 (ZCWPW1). The zf-CW domain adopts a new fold in which a zinc ion is coordinated tetrahedrally by four conserved Cys ligand residues. The tertiary structure of the zf-CW domain partially resembles that adopted by the plant homeo domain (PHD) finger bound to the histone tail, suggesting that the zf-CW domain and the PHD finger have similar functions. The solution structure of the complex of the zf-CW domain with the histone H3 tail peptide (1-10) with trimethylated K4 clarified its binding mode. Our structural and biochemical studies have identified the zf-CW domain as a member of the histone modification reader modules for epigenetic regulation.

INTRODUCTION

The zinc finger CW (zf-CW) domain is a zinc-binding domain comprising about 60 amino acids. A sequence alignment revealed three tryptophan (Trp) and four cysteine (Cys) residues that are conserved in the zf-CW family (the name zf-CW is derived from the conserved Cys and Trp residues) (Perry and Zhao, 2003). Especially, the four Cys residues are invariant among the amino acid sequences of the putative zf-CW domains, and they can potentially coordinate a zinc ion (Figure 1). The first two Cys residues are separated by two or four amino acids, as in classical zinc fingers. However, the arrangement of the third and fourth Cys residues is unusual, in that they are separated by 6–15 residues. Therefore, the zf-CW domain is classified as a new four cysteine zinc finger motif.

The function of the zf-CW domain is unknown, but the domain is frequently associated with chromatin-related factors (Perry

and Zhao, 2003). zf-CW domains have been identified in several enzymes that are involved in the control of the methylation states of the histone H3 tail.

The *Arabidopsis* SDG8 (SET domain group 8) protein is a member of the histone-lysine N-methyltransferase family, and specifically catalyzes the methylation of residue K36 in the histone H3 tail. The methylation promotes the expression of the flowering locus C (FLC) protein, an essential transcriptional repressor involved in controlling flowering time in *Arabidopsis* and preventing early flowering (Grini et al., 2009; Xu et al., 2008; Zhao et al., 2005). Besides the canonical AWS, SET, and post-SET domains that are characteristic of the SDG proteins, SDG8 contains an additional zf-CW domain, which is located upstream of the AWS domain. SDG8 could function by recognizing other modifications on the histone tail and/or DNA by the zf-CW domain.

A zf-CW domain was also found in the recently discovered lysine-specific demethylase LSD2/KDM1B, a homolog of LSD1/KDM1 (Karytinos et al., 2009). LSD1/KDM1 represses transcription by the demethylation of the mono- and dimethylated residue K4 in the histone H3 tail (Shi et al., 2004) (In this paper, we denote the amino acid residues of histone peptides with one-letter codes and those of the zf-CW domain with three-letter codes). LSD2/KDM1B also specifically demethylates the mono- and dimethylated K4 of the histone H3 tail and contributes to establishing DNA methylation imprints during oogenesis (Ciccone et al., 2009; Karytinos et al., 2009). Therefore, it is likely that LSD2/KDM1B also regulates chromatin structure through epigenetic signals, such as histone and/or DNA methylation.

In addition, the zf-CW domain is also observed in other proteins, besides the methylation or demethylation enzymes. MORC (microrchidia) family members are characterized by a conserved domain architecture consisting of a GHL (Gyrase B, Hsp90 and MutL) ATPase domain at the amino terminus, a zf-CW domain, a nuclear localization signal (NLS), and coiled-coil domains at the carboxy terminus (Iyer et al., 2008). The MORC family proteins are required for meiotic nuclear division in animals and perform chromatin remodeling by DNA superstructure manipulation in response to epigenetic signals, such as histone and/or DNA methylation (Iyer et al., 2008). Taken
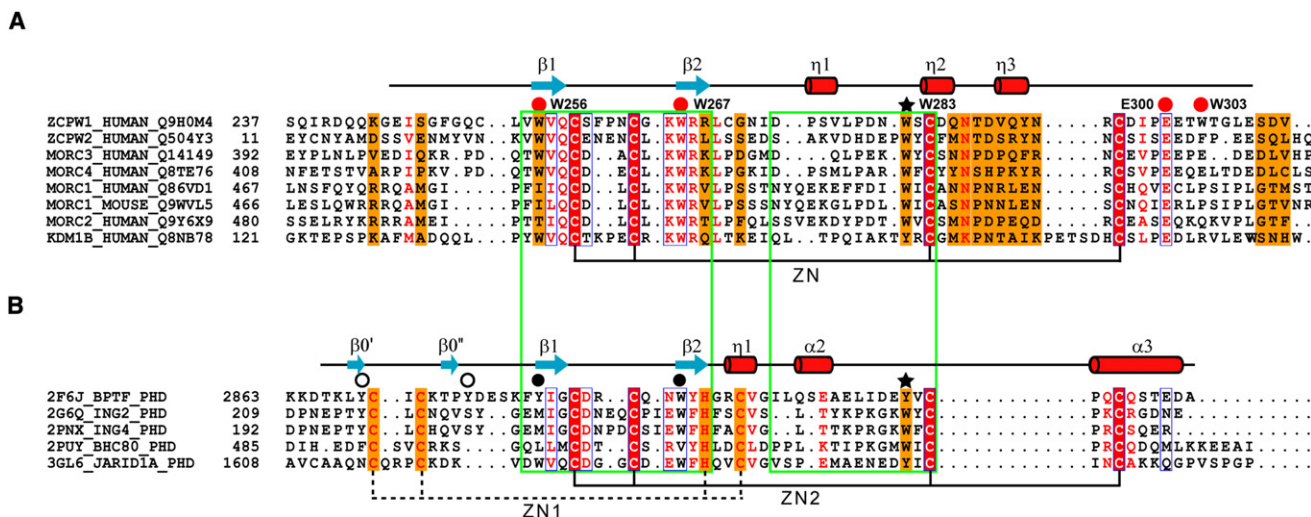
Figure 1. Sequence Alignment of the zf-CW Domains from Selected zf-CW Domain Containing Proteins and PHD Fingers from BPTF, ING2, ING4, BCH80, and JARID1A

Secondary structure elements of the human ZCWPW1 zf-CW domain (A) and the BPTF PHD finger, together with the zinc-binding modes, are shown. The conserved Trp cage forming residues are marked by closed red circles for the zf-CW domain and closed black circles for the PHD fingers (B), and partially conserved residues in PHD fingers are marked by open circles. Strictly conserved aromatic residues that stabilize the fold by hydrophobic interactions are marked by stars. Regions with homologous structures in the zf-CW domains and the PHD fingers are indicated by green frames.

together, these findings suggested that the zf-CW domains are involved in chromatin regulation through the recognition of epigenetic signals.

The modification states of the N-terminal histone H3 and H4 tails are linked to both transcriptional activation and repression, and they are regulated by a combinatorial network mediated by several protein motifs. For example, the PHD finger and royal superfamily members (chromo domain, tudor domain, and MBT domain) recognize methylated histones (for reviews, see Adams-Cioaba and Min (2009) and Taverna et al. (2007)). However, there was no information about the zf-CW domains, as sequence alignments did not reveal any significant homology with protein domains of known structure or function. Thus, the structure and function of the zf-CW domain in epigenetic control remained to be elucidated.

Here, we report the first three-dimensional structure of a zf-CW domain, comprising residues E246–E307 of the zf-CW and PWWP domain containing protein 1 (ZCWPW1) from *Homo sapiens*, determined by solution NMR spectroscopy. There is no functional information available for ZCWPW1. However, the PWWP domain is also known to be involved in epigenetic regulation (Wang et al., 2009b). Therefore, structural information about the zf-CW domain of ZCWPW1 may also provide general information about the function of the zf-CW domain in epigenetic control. We found structural similarity between the zf-CW domain and the PHD finger, which plays an important role in the recognition of the histone H3 tail. Further NMR experiments revealed the specific interactions between the ZCWPW1 zf-CW domain and the histone H3 tail peptide (1–10) with trimethylated K4. The present study provides evidence for the putative function of the zf-CW domain as a new histone modification reader.

RESULTS AND DISCUSSION

NMR Spectra and Structure Calculation

To determine the solution structure of the zf-CW domain, we measured a complete set of standard 2D and 3D NMR spectra (Clore and Gronenborn, 1994). The 2D [^{1}H,^{15}N]-HSQC spectrum of the zf-CW domain showed dispersed, sharp NH signals with similar intensities, which are characteristic of a folded protein (Figure 2). The resonance assignments of the polypeptide backbone and the nonlabile side-chain protons are complete, except for the amide protons of Cys253, Leu254, Trp256, and Asn273. Although some minor peaks were observed in the spectra, the resonances did not yield any substantial NOEs. Therefore, we excluded these resonances from the structural analysis.

The zinc coordination by the four Cys ligand residues, Cys259, Cys264, Cys285, and Cys296, was confirmed by the chemical shifts of their C$^\beta$ atoms, which were between 30.43 and 32.46 ppm, consistent with the sulfur groups coordinating a zinc ion (Lee et al., 1992). Correspondingly, a structure calculation based on the NOE restraints alone also showed that these four Cys ligand residues are clustered and oriented to coordinate one zinc ion. Therefore, we determined the solution structure in the presence of one zinc ion, coordinated by Cys259, Cys264, Cys285, and Cys296.

More than 20 NOE distance restraints per residue, including 375 long-range distance restraints as well as the restraints for coordinating the zinc ion, were used in the final structure calculations with the program CYANA 2.1 (Güntert, 2004). The final structures were energy-refined with the program AMBER9 (Case et al., 2005). The final 20 energy-minimized conformers that represent the solution structure of the ZCWPW1 zf-CW

Figure 2. 2D [^{1}H,^{15}N]-HSQC Spectrum of the zf-CW Domain of Human ZCWPW1

The spectrum was recorded at a ^{1}H frequency of 800 MHz (pH 7.0) and 298 K. Cross-peaks are labeled with the residue numbers. Side-chain resonances of asparagine and glutamine residues are indicated by horizontal lines.

domain are well defined and show excellent agreement with the experimental data (Table 1). The precision of the structure is characterized by RMSD values to the mean coordinates of 0.22 Å for the backbone and 0.59 Å for all heavy atoms, excluding the unstructured regions of residues 246–253 and 302–307 at the chain termini (Figure 3A). The quality of the structure is also reflected by the fact that 86.8% of the (ϕ,ψ) backbone torsion angle pairs were found in the most favored regions and 13.2% were within the additionally allowed regions of the Ramachandran plot, according to the program PROCHECK_NMR (Laskowski et al., 1996).

Tertiary Structure of the zf-CW Domain

The ZCWPW1 zf-CW domain structure starts with an N-terminal β-hairpin (β1: Trp256–Gln258, β2: Trp267–Arg269). The first and second zinc ligand residues, Cys259 and Cys264, are located at the tip of the β-hairpin. It is followed by an extended stretch that runs to the third Cys ligand residue, Cys285, and is associated with the β-hairpin. The successive 10-residue region connecting the third and fourth zinc ligand residues, Cys285 and Cys296, adopts a loop structure that is also associated with the β-hairpin. The C-terminal extension after the fourth zinc ligand residue, Cys296, lies on the loop structure between Cys 285 and Cys296, and turns toward the upper surface of the β-hairpin. Apart from the β-hairpin, there are no other regular secondary elements, except for three one-turn 3$_{10}$-helices (η1: Pro276–Val278, η2: Cys285–Gln287, and η3: Val291–Tyr293) (Figures 1, 3A, and 3B). Consequently, the ZCWPW1 zf-CW domain binds one zinc ion by its four conserved Cys ligand residues (Cys259, Cys264, Cys285, and Cys296), to form a compact globular fold that does not resemble any of the known zinc finger structures (Figure 3).

Apart from the conserved four Cys ligand residues, three Trp residues (Trp256, Trp267, and Trp283) are well conserved among all of the subgroups of the zf-CW domains (Perry and Zhao, 2003) (Figure 1). The first two Trp residues (Trp256 and

Trp267) are located on the surface of the β-hairpin where the two aromatic side chains face each other to form a cage, which is hereafter referred to as the Trp cage (Figure 3B). The third conserved Trp residue (Trp283) is located two sequence positions before the third Cys ligand residue under the β-hairpin, where it interacts with the hydrophobic residues Val257, Leu279, and Pro280 to stabilize the fold. Accordingly, the structure of the extended stretch, spanning residues 271–285, is fixed and forms a shallow hydrophobic pocket on the surface of the zf-CW domain with the β1 strand (Figure 3B).

The zf-CW domain contains the highly conserved Lys266-Trp267-Arg268 sequence on the β2 strand (Figure 1). The guanidyl group of Arg268 occupies the space between the β2 strand and the C-terminal extension after the fourth Cys ligand residue, and hydrogen bonds to the carboxyl oxygens of Ile298 and Pro299 in the C-terminal extension, thus turning the C terminus back (Figure 3C). The positively charged side chain of Lys266 is in close proximity to the negatively charged side chain of Glu300. The electrostatic interactions between Lys266 and Arg268 and their counterparts seem to be necessary for the association of the C-terminal extension with the β2 strand (Figure 3C). Consequently, the negatively charged side chains of Glu300 and Glu301 as well as the aromatic side chain of Trp303 are in proximity to the Trp cage on the β-hairpin (Figure 3B).

Structural Similarity of the zf-CW Domain to PHD Fingers

As described above, the zf-CW domains contain well-conserved Cys and Trp residues. Accordingly, the canonical zf-CW domain has the characteristic Cys-X-X-Trp and Trp-X-Cys sequence motifs, which contain the second and third Cys ligand residues, respectively. Sequence comparisons with other zinc finger domains revealed homologous sequence motifs in several PHD fingers. For example, the BPTF PHD finger (Li et al., 2006), the ING2 PHD finger (Pena et al., 2006), and the JARID1A PHD finger (Wang et al., 2009a), as shown in Figure 1.

The canonical PHD fingers have the CCCC-CHCC motif and bind to two zinc ions in a cross-brace manner. Although the zf-CW domain does not belong to the cross-brace zinc finger protein family (Figure 1), we tried to compare the zf-CW domain and the BPTF PHD finger from a structural point of view.

The main chain structures of the conserved Cys-X-X-Trp and Trp-X-Cys sequence motifs in the zf-CW domain could be

Table 1. Structural Statistics for the Free zf-CW Domain and the zf-CW-H3$_{(1-10)}$K4me3 Complex of Human ZCWPW1

	Free	Complex
Conformational Restraints		
NOE distance restraints		
Total	1263	1506
Intraresidue	314	345
Sequential ($|i - j| = 1$)	341	401
Medium-range ($1 < |i - j| < 5$)	233	258
Long-range ($|i - j| \geq 5$)	375	502
ϕ/ψ dihedral angle restraints from TALOS	13/13	13/13
Hydrogen bond restraints (upper/lower)	2/2	8/8
Intermolecular NOEs	—	117
Intramolecular NOEs for H3$_{(1-10)}$K4me3	—	72
Structure Statistics		
CYANA target function (Å^2)	0.10	0.44
Residual NOE violations		
Number >0.1 Å	0	1
Maximum (Å)	0.04	0.18
Residual dihedral angle violations		
Number >2.5°	0	0
Maximum (°)	0.53	1.31
Energies (kcal/mol)		
Mean restraint violation energy	7.44	7.60
Mean AMBER energy	−2823	−3533
Ramachandran plot statistics (%)		
Residues in most favored regions	86.8	89.4
Residues in additional allowed regions	13.2	10.6
Residues in generously allowed regions	0.0	0.0
Residues in disallowed regions	0.0	0.0
Rmsd to mean coordinates (Å)		
Backbone	0.22	0.20
Heavy atoms	0.59	0.54

Ramachandran plot statistics and rmsd values are for residues Leu254-Glu301 of the zf-CW domain.

superimposed onto those of the corresponding sequence motifs in the BPTF PHD finger (Li et al., 2006) (Figure 4A). In addition, the side chains of the two above-mentioned Trp and Tyr residues in the BPTF PHD finger could be overlaid on those of the two corresponding Trp residues in the zf-CW domain (Figure 4A). Accordingly, the third, fourth, and seventh Cys ligand residues in the BPTF PHD finger are located at the positions corresponding to the first, second, and third Cys ligand residues in the zf-CW domain, respectively, and the position of the zinc ion in the zf-CW domain corresponded to that of the second zinc ion in the BPTF PHD finger (Figures 1, 4B, and 4E).

In the BPTF PHD finger, the side chain of Tyr51 in the Tyr-X-Cys sequence motif (indicated by a black star in Figure 1) contacts the hydrophobic amino acids on the β1 strand and on the segment between the sixth and seventh Cys ligand residues to form a shallow hydrophobic pocket (Figure 4A). The solution structure of the zf-CW domain indicated that Trp283 in the Trp-X-Cys sequence motif plays the same role as Tyr51

in the BPTF PHD finger (Figure 4A). Accordingly, the extended stretch spanning residues 271–285 in the zf-CW domain could be superimposed roughly on the corresponding region of the BPTF PHD finger (Figure 4A). In other PHD fingers, aromatic amino acid residues are conserved at the position corresponding to Tyr51 in the BPTF PHD finger (Figure 1), and similar shallow hydrophobic pockets are observed on the surface of these PHD fingers (Figures 4C and 4D). Therefore, we concluded that zf-CW domains and PHD fingers share a homologous substructure, composed of the core β-hairpin and the extended stretch (Figures 1 and 4B), and that the zf-CW domain is more closely related to the PHD finger than to other known zinc fingers (Figure 4). Furthermore, it is conceivable that the similar shallow hydrophobic pocket on the surface of the zf-CW domain could accommodate a similar target group as the PHD fingers.

The N-terminal peptide of the histone H3 tail fits well into this shallow hydrophobic pocket of the PHD fingers. In addition, as reported for the PHD finger domains from BPTF (Li et al., 2006) (Figure 4A), ING2 (Pena et al., 2006) (Figure 4C), and JARID1A (Wang et al., 2009a) (Figure 4D), the PHD fingers that have a Cys-X-X-Trp sequence motif (corresponding to the β2 strand) recognize the histone H3 tail with trimethylated K4. Taken together, these findings suggest that the zf-CW domain may be related to the recognition of the histone H3 tail with methylated Lys residues.

On the other hand, there are two distinctive differences between the zf-CW domain and the PHD fingers. First, the zf-CW domain lacks the zinc knuckle structure observed in the PHD fingers (β0′ and β0″ in Figure 1). Therefore, the zf-CW domains lack the first zinc-binding site provided by the zinc knuckle in the PHD finger (Figures 1 and 4B). Second, the peptide segment after the third Cys ligand residue of the zf-CW domain adopts a distinct structure (Figure 4). In the PHD fingers, the seventh and eighth Cys ligand residues are separated by two amino acids. The C-terminal regions after the eighth Cys ligand residue of the PHD fingers are located under the β-hairpin and point away from the core part of the structure (Figure 4). In contrast, the corresponding third and fourth Cys ligand residues in the zf-CW domain are separated by ten intervening residues, and no α-helical structure exists after the last Cys ligand residue (Figure 4).

Consequently, the zf-CW domain and the PHD finger have a common core structure, composed of the β-hairpin and the extended stretch, which could potentially bind to the histone H3 tail with methylated K4 (Figures 1 and 4B). However, the N-terminal and C-terminal segments attached to the core region adopt different structures in the two domains (Figure 4).

Titration of the zf-CW Domain with Histone Tail Peptides

As described above, the posttranslationally modified histone H3 tail is a putative target of the zf-CW domain. To examine whether the zf-CW domain could bind to the N-terminal tail regions of histones H3 and/or H4, we performed 2D [^{1}H,^{15}N]-HSQC titration experiments with N-terminal 20-residue peptides from histone H3, either nonmethylated (H3$_{(1-20)}$K4me0) or with dimethylated K4 (H3$_{(1-20)}$K4me2), trimethylated K4 (H3$_{(1-20)}$K4me3), and trimethylated Lys9 (H3$_{(1-20)}$K9me3), as well as the N-terminal
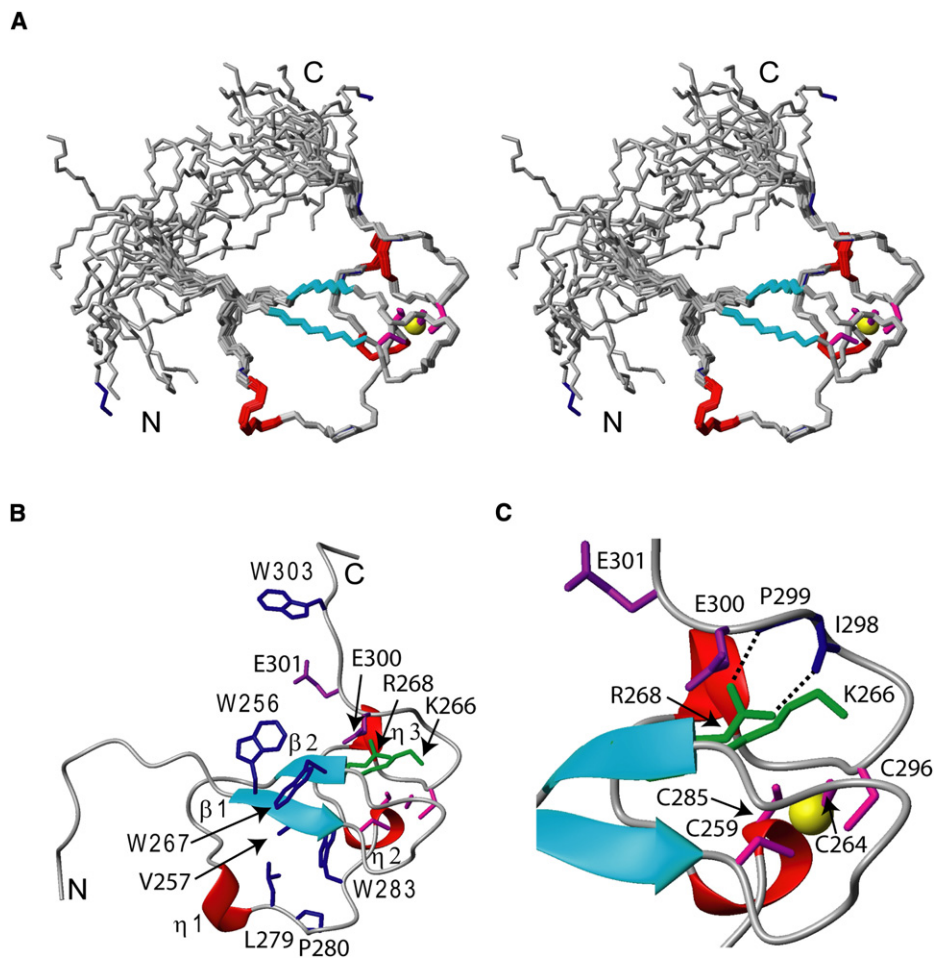
Figure 3. Solution Structure of the zf-CW Domain of Human ZCWPW1

(A) Stereo view of backbone traces of the 20 conformers of the solution structure of the free zf-CW domain (residues 246–307). Secondary structure elements are colored. The side chains of the zinc-binding residues are shown in magenta.

(B) Ribbon representation with strongly conserved residues.

(C) Ribbon representation with residues associated with the C-terminal extension. Color coding: β strands, cyan; 3$_{10}$-helices, red; zinc, yellow; zinc-binding residues, magenta; hydrophobic residues, blue; positively charged residues, green; negatively charged residues, purple.

20-residue peptide of the histone H4 tail with trimethylated K20 (H4$_{(1-20)}$K20me3).

When we compared the effects of titrating several histone H3 peptides on the zf-CW domain, similar tendencies of the chemical shift changes were observed for all of the H3 tail peptides, and the perturbed residues of the zf-CW domain could be identified (Figure 5). The smallest chemical shift changes among the examined peptides were observed for H3$_{(1-20)}$K4me0, suggesting that it is in fast exchange on the NMR timescale. The magnitudes of the chemical shift changes for H3$_{(1-20)}$K4me2 and H3$_{(1-20)}$K9me3 were greater than those for H3$_{(1-20)}$K4me0. Furthermore, the effect of H3$_{(1-20)}$K4me3 was prominent among these peptides derived from the histone H3 tail, and some resonances exhibited medium exchange behavior (see Figure S1 available online).

Some resonances were missing in the free form of the zf-CW domain. Interestingly, upon the addition of H3$_{(1-20)}$K4me3, new resonances from Cys253, Leu254, Trp256, and Asn273 emerged in the spectra. This suggests that the dynamics of

these residues in the zf-CW domain were affected upon binding to H3$_{(1-20)}$K4me3.

Most of the affected residues are in the region Leu254–Cys285, which shares structural homology with the PHD finger. In addition, Glu301, Trp303, Leu306, and Glu307, in the C-terminal extension after the fourth Cys ligand residue, were also affected. In the case of the PHD finger, the C-terminal region following the last Cys ligand residue is not responsible for the recognition of the H3 trimethylated K4 peptide. Therefore, the influence on the C-terminal segment by H3$_{(1-20)}$K4me3 is specific for the zf-CW domain.

The addition of H4$_{(1-20)}$K20me3 to the zf-CW domain induced chemical shift changes in the [^{1}H,^{15}N]-HSQC spectrum of the zf-CW domain with a similar magnitude as those for H3$_{(1-20)}$K4me0. Taken together, the characteristics of the chemical shift changes in the titration experiments with the different histone peptides suggested that the histone H3 tail with trimethylated K4 is the preferred target for the ZCWPW1 zf-CW domain (Figure 5).
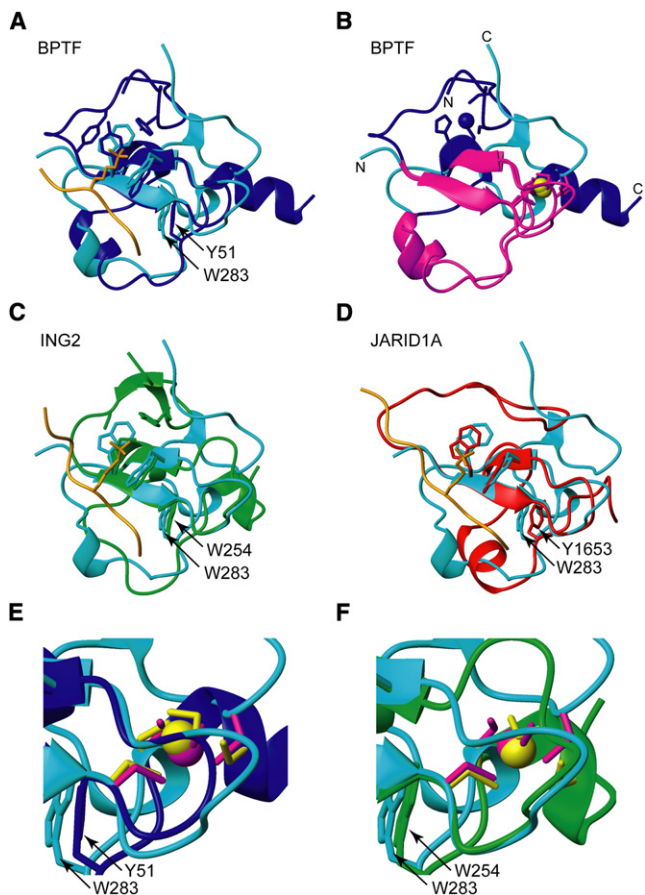
Figure 4. Structure Comparison of the Human ZCWPW1 zf-CW Domain with Selected PHD Fingers

Superpositions of the free zf-CW domain (cyan) with PHD fingers, showing the residues forming the aromatic cage and the H3K4me3 peptide (orange).
(A) BPTF (blue).
(B) BPTF, showing the region with a homologous structure in the zf-CW domain and the BPTF PHD finger (magenta).
(C) ING2 (green).
(D) JARID1A (red).
(E and F) Close-up views of the zinc coordination site between zf-CW and the BPTF PHD (E) and ING2 PHD (F) fingers.

Figure 5. Chemical Shift Perturbations of the Human ZCWPW1 zf-CW Domain upon the Addition of Several Histone Tail Peptides

H3K4me0 (A), H3K4me2 (B), H3K4me3 (C), H3K9me3 (D), and H4K20me3 (E). The chemical shift changes were estimated from the spectrum of the zf-CW domain (0.1 mM) and that with a 1:3 molar ratio of peptide. The weighted backbone amide chemical shift changes in the 2D [^{1}H,^{15}N]-HSQC spectra, $\Delta\delta$, were calculated according to the equation $\Delta\delta = ((\Delta HN)^2 + (\Delta N/6.5)^2)^{1/2}$. Resonances with weighted backbone amide chemical shift changes above the mean value (continuous red line) plus 1 SD (dashed red line) are labeled. Unassigned residues and residues with signals that disappeared during the titration are marked by black and red closed circles, respectively. Proline residues are marked by black stars. See also Figure S1.

Isothermal Titration Calorimetry Experiments for the Binding of the zf-CW Domain to the Histone H3 Tail Peptides

In order to investigate whether the zf-CW domain discriminates the different methylation states of K4 in the histone H3 tail, we focused on the shorter 10-residue peptide of the N-terminal histone H3 tail. Namely, we compared the binding activities of the zf-CW domain for the respective peptides with nonmethylated K4 (H3$_{(1-10)}$K4me0), monomethylated K4 (H3$_{(1-10)}$K4me1), dimethylated K4 (H3$_{(1-10)}$K4me2), trimethylated K4 (H3$_{(1-10)}$K4me3), and trimethylated Lys9 (H3$_{(1-10)}$K9me3) by isothermal titration calorimetry (ITC) measurements. Consistent with the results of the NMR titration experiments, the zf-CW domain bound to H3$_{(1-10)}$K4me3 with a K_d value of 16.7 μM. Meanwhile, the K_d values for H3$_{(1-10)}$K4me2, H3$_{(1-10)}$K4me1, and H3$_{(1-10)}$K4me0 were 41.8, 91.7, and 235 μM, respectively (Table 2;

Figure S2). In agreement with the NMR titration experiments, the binding of H3$_{(1-10)}$K4me0 was 14 times weaker than that of H3$_{(1-10)}$K4me3. Increasing the methylation level of the K4 residue thus strengthened the binding of the zf-CW domain to the histone H3 tail. On the other hand, the K_d value for

Table 2. Binding Affinities of the zf-CW Domain and the PHD Fingers to H3$_{(1-10)}$K4me Peptides by ITC Experiments

Protein	Ligand	Kd (μM)
zf-CW wild type	H3$_{(1-10)}$K4me3	16.7 ± 0.3
zf-CW wild type	H3$_{(1-10)}$K4me2	41.8 ± 0.7
zf-CW wild type	H3$_{(1-10)}$K4me1	91.7 ± 6.5
zf-CW wild type	H3$_{(1-10)}$K4me0	234.7 ± 2.3
zf-CW W303E	H3$_{(1-10)}$K4me3	28.3 ± 0.7
zf-CW W303E	H3$_{(1-10)}$K4me0	297.6 ± 49.6
zf-CW W303A	H3$_{(1-10)}$K4me3	105.0 ± 11.3
zf-CW W303A	H3$_{(1-10)}$K4me0	298.0 ± 94.4
zf-CW E300A	H3$_{(1-10)}$K4me3	87.0 ± 4.4
zf-CW E300A	H3$_{(1-10)}$K4me0	No binding
zf-CW W256I/E301R/T302L/W303P	H3$_{(1-10)}$K4me3	No binding
zf-CW W256I/E301R/T302L/W303P	H3$_{(1-10)}$K4me0	No binding
JARID1A PHD (Wang et al., 2009a)	H3$_{(1-10)}$K4me3	0.75 ± 0.04[ITC]
JARID1A PHD (Wang et al., 2009a)	H3$_{(1-10)}$K4me0	20.7 ± 1.0[ITC]
BPTF PHD (Li et al., 2006)	H3$_{(1-10)}$K4me3	1.6 ± 0.1[FP]/2.7[ITC]
BPTF PHD (Li et al., 2006)	H3$_{(1-10)}$K4me0	No binding
ING2 PHD (Pena et al., 2006)	H3$_{(1-10)}$K4me3	1.5 ± 1[FP]
ING2 PHD (Pena et al., 2006)	H3$_{(1-10)}$K4me0	2240 ± 350[FP]
BHC80 PHD (Lan et al., 2007)	H3$_{(1-10)}$K4me0	33 ± 6.4[ITC]
JMJD2A tudor (Huang et al., 2006)	H3$_{(1-10)}$K4me3	10.4[SPR]
JMJD2A tudor (Huang et al., 2006)	H3$_{(1-10)}$K4me0	n/d[SPR]
CHD1 Chromo (Flanagan et al., 2005)	H3$_{(1-10)}$K4me3	38[ITC]/5[FP]
CHD1 Chromo (Flanagan et al., 2005)	H3$_{(1-10)}$K4me0	n/d[FP]
L3MBTL1 MBT (Li et al., 2007)	H3$_{(1-10)}$K4me2	75 ± 12[FP]

The data for the zf-CW domains were obtained from ITC experiments. Data for other proteins are from the given reports and were obtained from fluorescence polarization (FP), ITC, or surface plasmon resonance (SPR) experiments, as indicated in the last column. See also Figures S2 and S4.

H3$_{(1-10)}$K9me3 was 271 μM, which was almost equal to that for H3$_{(1-10)}$K4me0. Therefore, we concluded that the zf-CW domain preferentially binds to the histone H3 tail with trimethylated K4, and that the trimethylated K4 is the key residue for the binding.

Complex Structure of the zf-CW Domain and the H3$_{(1-10)}$K4me3 Peptide

The NMR titration and ITC experiments indicated that the N-terminal peptide of the histone H3 tail with the trimethylated K4 is the putative target of the zf-CW domain. Therefore, we solved the NMR solution structure of the complex between the zf-CW domain and the H3$_{(1-10)}$K4me3 peptide.

To determined the complex structure, filtered 2D COSY, TOCSY, and NOESY experiments as well as standard triple resonance experiments were performed for mixtures of the zf-CW domain and the H3$_{(1-10)}$K4me3 peptide, with molar ratios of 1:0.5, 1:1, and 1:3, respectively. For the structure calculation, we mainly utilized the NOESY spectra for the mixture of the zf-CW domain and the H3$_{(1-10)}$K4me3 peptide with a 1:1 molar

ratio. With the help of the filtered NOESY experiments (Figure S3), 117 intermolecular NOE distance restraints between the zf-CW domain and the H3$_{(1-10)}$K4me3 peptide were identified and used for the structure calculation of the complex between the zf-CW domain and the H3$_{(1-10)}$K4me3 peptide (Figure 6).

In the complex structure, the H3$_{(1-10)}$K4me3 peptide forms a three-stranded anti-parallel β sheet together with the two β strands of the zf-CW domain (Figure 6B). The intermolecular NOE network suggested the presence of several hydrogen bonds between the main chain of the H3$_{(1-10)}$K4me3 peptide and the first β strand of the zf-CW domain, i.e., between the carbonyl oxygen of R2 and the amide proton of Gln258, the amide proton of K4 and the carbonyl oxygen of Trp256, the carbonyl oxygen of K4 and the amide proton of Trp256, and the carbonyl oxygen of T6 and the amide proton of Leu254. The N-terminal amino group of A1 in H3$_{(1-10)}$K4me3 interacts with the carbonyl oxygen and the O^{δ1,2} atoms of Asp280 in the zf-CW domain. The β-methyl moiety of A1 fits into the shallow pocket formed by the extended stretch spanning residues 271–285 and the first β strand in the zf-CW domain, and the shallow pocket also accommodates the γ-methyl moiety of the T3. The side chains of R2 and Gln258 on the β1 strand are aligned side by side, suggesting the existence of a hydrogen bond between O^{ε1} of Gln258 and the guanidyl group of R2. The trimethylated side chain of K4 interacts with the Trp cage formed by Trp256 and Trp267 on the β-hairpin, as well as Trp303 from the C-terminal extension through cation-π interactions (Figures 6C and 6D). In addition, the negatively charged side chain of Glu300 is located between the aromatic side chains of Trp267 and Trp303 to attract the positive charge of the trimethylated K4 through electrostatic interactions. At the same time, the expansive aromatic cage also accommodates the γ-methyl group of T6 (Figures 6C and 6D). The structures of the free and bound zf-CW domain are quite similar, except for the C-terminal region following Glu300, which adapted its structure when recognizing the trimethylated K4 (Figures 6E and 6F). On the other hand, in the case of the PHD fingers, the N-terminal zinc knuckle, which is missing in the zf-CW domain, is involved in the formation of the aromatic cage for the trimethylated K4 (Figure 4). In conclusion, the complex structure clearly explains how the histone H3 tail, with the trimethylated K4, fits to the ZCWPW1 zf-CW domain through specific interactions, including cation-π and electrostatic interactions (Figures 6C and 6D) and suggests that the histone H3 tail, with the trimethylated K4, could be the true target of the ZCWPW1 zf-CW domain.

Dynamic Properties of the zf-CW Domain

To discuss the dynamic properties of the zf-CW domain upon binding to H3$_{(1-10)}$K4me3, the ^{15}N R_1, R_2 relaxation rates and the steady-state ^{1}H-^{15}N NOEs were measured for the zf-CW domain at 25°C (Figure 7). Overlapped resonances and resonances with a poor signal-to-noise ratio (S/N) were excluded from the relaxation analysis. In the case of the free form, the average NOE values for the β-hairpin (residues 254–271) and the region spanning residues 285–300 (the region following the third Cys ligand residue) were about 0.81. These values are in agreement with the result that the β-hairpin and the region spanning residues 285–300 are tightly packed to form a rigid body in solution. The NOE values for the N- and C-terminal extensions
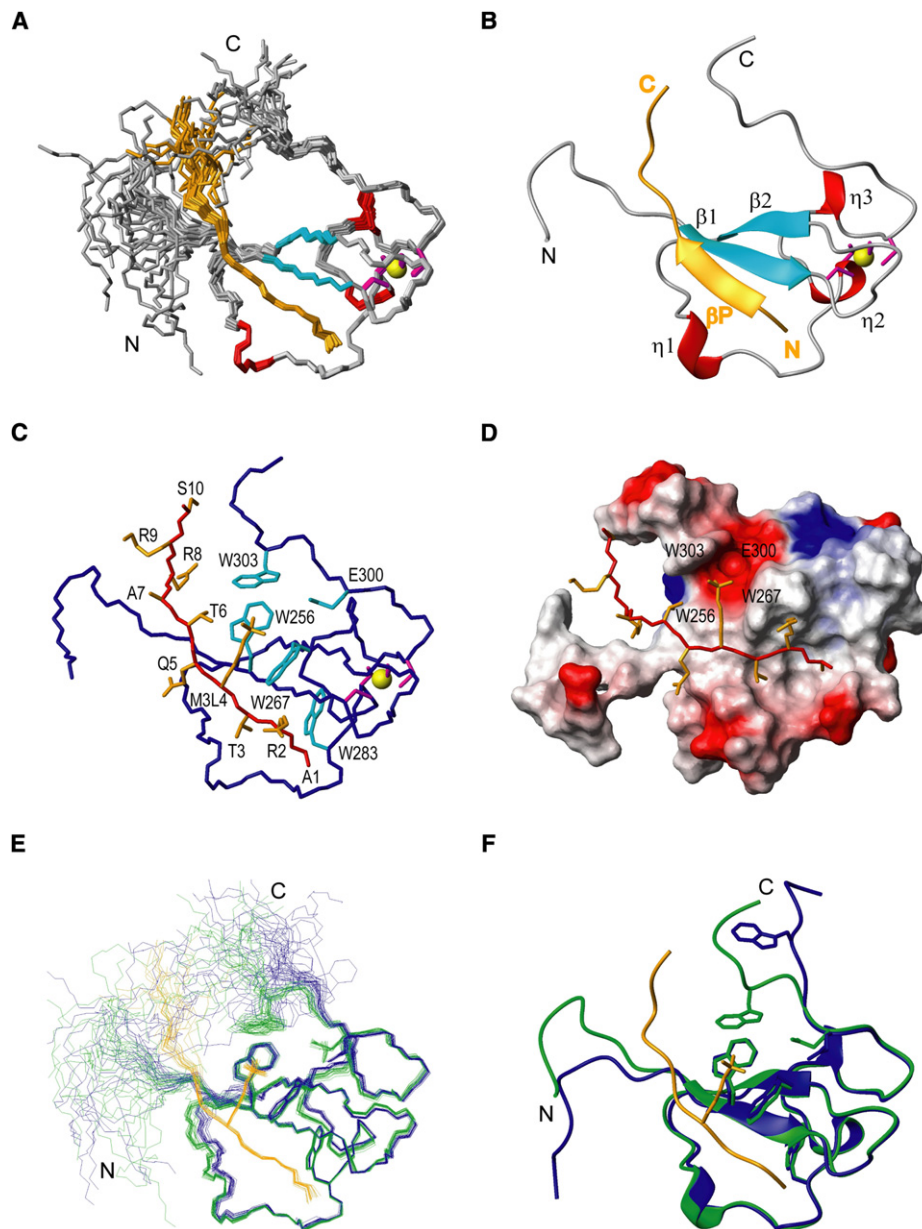
Figure 6. Solution Structure of the Human ZCWPW1 zf-CW- H3$_{(1–10)}$K4me3 Complex

(A) Backbone traces of the 20 conformers of the solution structure.

(B) Lowest energy structure, in a ribbon representation.

(C) The zf-CW domain and the H3$_{(1–10)}$K4me3 peptide are shown in stick representations.

(D) Electrostatic surface potential of the zf-CW domain in complex with H3$_{(1–10)}$K4me3.

(E) Superposition of the 20 conformers of the solution structures of the free and complexed zf-CW domains.

(F) Superposition of the lowest energy structures of the free and complexed zf-CW domains.

See also Figure S3.

(residues 246–254 and 303–307, respectively) decreased gradually when approaching the chain termini, indicating that these regions are flexible in solution. Interestingly, the NOE values for the region spanning residues 271–281 were also smaller than those for the above-mentioned rigid core (Figure 7). Upon complex formation, the lowered NOE values for residues 278–281 increased slightly, while they decreased further for Trp283.

The region spanning residues 278–281 is responsible for the recognition of A1 and T3 in the H3$_{(1–10)}$K4me3 peptide. Thus, it is conceivable that the interactions with the N-terminal portion of H3$_{(1–10)}$K4me3 stabilize the structure of the region encompassing residues 278–281, while the mobility was induced for Trp283. On the other hand, the motion of the Trp303 amide group in the C-terminal extension of the zf-CW domain was
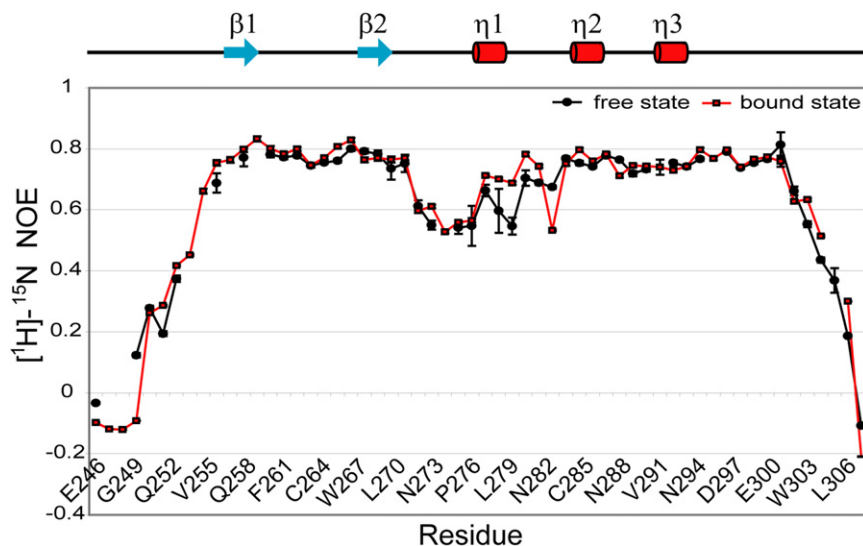
Figure 7. Heteronuclear ^{1}H-^{15}N NOE Data of the Free and Bound Forms of the Human ZCWPW1 zf-CW Domain

The backbone heteronuclear ^{1}H-^{15}N NOEs of the zf-CW domain in the free form (closed circles) and in complex with H3$_{(1-10)}$K4me3 (open squares) are plotted against the amino acid sequence. Secondary structure elements are indicated at the top. The heteronuclear NOE errors were estimated from the rms value of the baseline noise in the NOE and reference spectra (Farrow et al., 1994).

slightly restricted in the presence of H3$_{(1-10)}$K4me3, reflecting the result that Trp303 of the ZCWPW1 zf-CW domain is involved in the recognition of the trimethylated K4.

The Binding Mode for the Histone H3 Tail with Methylated K4 in Other Recognition Domains

In the case of the ZCWPW1 zf-CW domain, the Trp cage, supplemented by Trp303 and the conserved, negatively charged residue Glu300, participates in the recognition of the trimethylated K4 and the methyl moiety of T6 (Figure 8A). As described above, the core structure is shared between the zf-CW domain and the PHD fingers. However, several PHD fingers utilize various types of aromatic cages for the recognition of trimethylated K4 that are distinct from that of the zf-CW domain. For example, the rigid aromatic cages of the BPTF and ING2 PHD fingers could fit well with the trimethylated K4 of the histone H3 tail (Li et al., 2006; Pena et al., 2006) (Figures 8B and 8C). The common feature of the BPTF and ING2 PHD fingers is that the aromatic amino acid residues located in the zinc knuckle are involved in the formation of the aromatic cage. The fixed space of the aromatic cage strictly discriminates the methylation levels of K4. In the case of the ING2 PHD finger, the aromatic cage is not perfect, as compared with that of the BPTF PHD finger, because the Tyr residue that shapes a side surface of the aromatic cage in BPTF is replaced by a Ser residue in ING2 (Pena et al., 2006) (Figure 8C). The discrimination of the methylation levels by the ING2 PHD finger is less strict than that by the BPTF PHD finger (Li et al., 2006; Pena et al., 2006). However, even in the case of the ING2 PHD finger, the ratio of the K_d values is about 1500-fold lower for trimethylated K4 than for nonmethylated K4. Instead, in the case of the zf-CW domain, the ratio is about 14-fold. Thus, in the BPTF PHD finger, the robust aromatic cage defines the space for the trimethyl moiety of K4, and enhances the strictness of the recognition.

On the other hand, the JARID1A PHD finger has a Trp cage similar to that of the zf-CW domain (Wang et al., 2009a) (Figure 8D), and only the cation-π interactions mediated by the Trp cage seems to anchor the trimethylated K4 and the methyl

moiety of T6. Unlike the BPTF and ING2 PHD fingers, the discrimination of the methylation levels by the JARID1A PHD finger is less strict, and the binding affinity difference is 28-fold between H3K4me3 and H3K4me0 (Wang et al., 2009a), which is comparable to that of the zf-CW domain. In the zf-CW domain, besides the Trp cage, the C-terminal extension contributes to the binding of the trimethylated K4. The flexibility of the C-terminal extension around Trp303 in the zf-CW domain, which was detected by the NMR dynamics measurements, may confer the broad binding selectivity for several histone H3 tail peptides, while the Trp cage mainly contributes to the recognition of the trimethylated K4.

Besides the PHD fingers, the royal superfamily members (Kim et al., 2006), such as the JMJD2A Tudor domain (Huang et al., 2006), the CHD1 chromo domain (Flanagan et al., 2005), and the MBT domains of L3MBTL1 (Li et al., 2007), are protein motifs that recognize the histone H3 tail with methylated K4. A detailed examination of the binding sites of these domains revealed that the aromatic cage, along with the negatively charged amino acids, constitutes the binding pocket for the methylated K4, and the spatial relationship between the aromatic cage and the negatively charged amino acids affects the specificity for the different methylation levels of the K4 residue. The aromatic cage of the JMJD2A Tudor domain is composed of three aromatic amino acids, including one Trp residue (Figure 8F), and that of the CHD1 chromo domain is composed of two Trp residues, as in the zf-CW domain (Figure 8G). In both cases, the aromatic cage plus the negatively charged amino acid preferentially recognized the trimethylated lysine residues, rather than the dimethylated ones (Flanagan et al., 2005; Huang et al., 2006). On the contrary, the MBT domain of L3MBTL1 binds to the dimethylated K4 histone peptide specifically with a similar aromatic cage plus a negatively charged amino acid residue (Li et al., 2007) (Figure 8H). In this case, the negatively charged amino acid residue was in closer proximity to the H$^\varepsilon$ proton of K4 than in the former cases. In the zf-CW domain, the spatial relationship between the Trp cage and the Glu300 was similar to that observed in the CHD1 chromo domain, reflecting the preference of the zf-CW domain. Taken together, the recognition mode of the zf-CW domain, mediated by an aromatic cage plus a negatively charged residue, is considered to be a common feature of the histone modification readers, and the zf-CW domain thus represents a new histone tail modification reader,
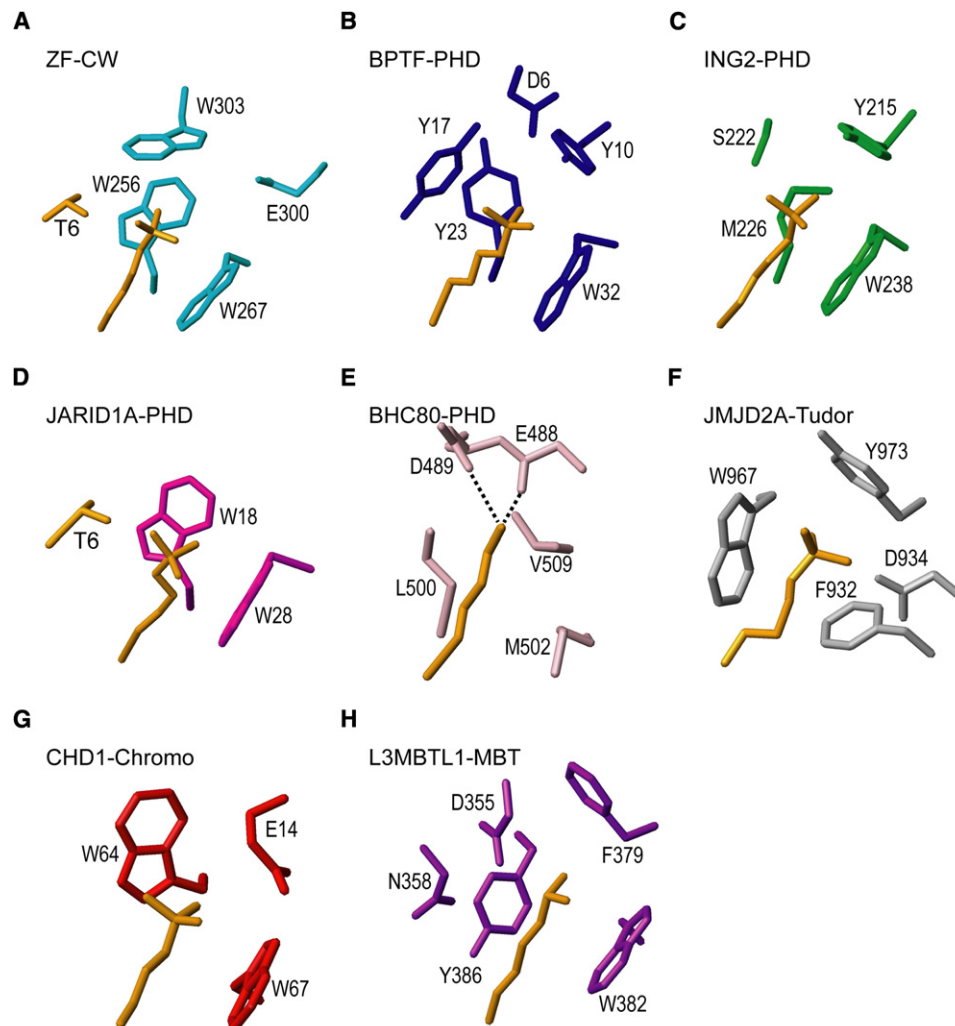
Figure 8. Comparison of the Trp Cage in the zf-CW Domain and Other Reader Modules for the Methylated K4 of the Histone H3 Tail
Side chains of the residues forming the Trp cage with the accommodated trimethylated, dimethylated, or nonmethylated K4 (orange) are shown.
(A) ZCWPW1 zf-CW domain.
(B) BPTF PHD finger.
(C) ING2 PHD finger.
(D) JARID1A PHD finger.
(E) BHC80 PHD finger.
(F) JMJD2A Tudor domain.
(G) CHD1 Chromo domain.
(H) L3MBTL1 MBT domain.

in addition to the known PHD fingers and the royal superfamily members.

Mutation Experiments with the ZCWPW1 zf-CW Domain
In the complex structure between the ZCWPW1 zf-CW domain and H3$_{(1-10)}$K4me3, two Trp residues (Trp256 and Trp267) in the β-hairpin are important for the accommodation of the side chain of the trimethylated K4. Among the other subgroup members of the zf-CW domain, Trp267 is perfectly conserved. Trp256 is highly conserved and only rarely replaced, namely by an Ile residue in the mouse MORC1 zf-CW domain (Figure 1). The BHC80 PHD finger lacks the aromatic cage on the β-hairpin, and the acidic residue in its binding site for K4 preferably binds

the histone H3 tail peptide with lower, rather than higher methylation levels (Lan et al., 2007) (Figure 8E). Thus, in order to confirm the importance of the Trp cage, and to examine the effect on the target recognition by the replacement of the Trp residue observed in the mouse MORC1 zf-CW domain, we made the quadruple mutant W256I/E301R/T302L/W303P of the ZCWPW1 zf-CW domain to resemble the mouse MORC1 zf-CW domain. The binding constants for H3$_{(1-10)}$K4me3 and H3$_{(1-10)}$K4me0 were measured by ITC experiments. We found that the quadruple mutant protein completely lost the binding affinity for H3$_{(1-10)}$K4me3 and H3$_{(1-10)}$K4me0. This suggests that the Trp cage on the β-hairpin is necessary for the recognition of the histone H3 tail peptide, with or without methylated K4, and

that, unlike the canonical zf-CW domain, the mouse MORC1 zf-CW domain may not recognize the histone H3 tail peptide.

In the case of the ZCWPW1 zf-CW domain, Glu300 and Trp303 in the C-terminal extension play a supplemental role in the recognition of the trimethylated K4 residue. In order to clarify the role of these auxiliary amino acids in the C-terminal extension, we first replaced Glu300 with Ala. The binding of the E300A mutant to the $H3_{(1-10)}K4me3$ peptide became nearly five times weaker than that of the wild-type protein, thus confirming that Glu300 has a supporting function in the recognition of the methylated histone peptide. Interestingly, the E300A mutant lost its binding activity to $H3_{(1-10)}K4me0$, indicating that the absolutely conserved, negatively charged Glu300 residue is required for binding to the nonmethylated histone H3 peptide. As described above, the discrimination between $H3_{(1-10)}K4me3$ and $H3_{(1-10)}K4me0$ by the zf-CW domains is not as strong as that by the BPTF and ING2 PHD fingers. If the role of the zf-CW domain is simply the discrimination of the trimethylated K4, then Glu300 might have been replaced by other nonpolar amino acid residues during evolution, although the binding to $H3_{(1-10)}K4me3$ would have become slightly weaker. The rather broad recognition by the zf-CW domain may have a biological role in epigenetic control, in contrast to the strict discrimination mediated by PHD fingers.

In some subgroup members of the zf-CW domain family, an acidic amino acid, rather than a hydrophobic one, occupies the position corresponding to Trp303 (Figure 1). In order to elucidate the role of Trp303, we prepared the mutants W303E and W303A and measured their binding affinities to $H3_{(1-10)}K4me3$ and $H3_{(1-10)}K4me0$ by ITC experiments. The binding affinities of the W303E mutant to $H3_{(1-10)}K4me3$ and $H3_{(1-10)}K4me0$ were only slightly weaker than those of the wild-type. Therefore, the replacement did not significantly affect the binding ability of the zf-CW domain. On the contrary, the binding of the W303A mutant to $H3_{(1-10)}K4me3$ was nearly six times weaker than that of the wild-type, whereas the binding of the W303A mutant to $H3_{(1-10)}K4me0$ was almost unaffected. This means that Trp303 has a supporting role in the recognition of the trimethylated K4, and it could be replaced by the acidic amino acid that was observed in the other zf-CW domain subgroups. We checked the 1D spectra for all of these mutant proteins described above, and excluded the possibility that protein unfolding affected the binding activity (Figure S4).

Conclusions

The present work has provided the first structural and biochemical information about the zf-CW domain. We found that the zf-CW domain is another building block in the repertoire of zinc-binding structural modules, and a new histone modification reader for the histone H3 tail with trimethylated K4. The present information provides a basis for understanding the epigenetic control mediated by the zf-CW domain.

EXPERIMENTAL PROCEDURES

Protein Sample Preparation

Then zf-CW domain (residues 246–307) from human ZCWPW1 was synthesized by a cell-free protein synthesis system (Kigawa et al., 2004; Matsuda et al., 2006) and purified as described previously (Matsuda et al., 2006). For

the structure determination, a single 1.1 mM uniformly ^{13}C- and ^{15}N-labeled sample was prepared in 20 mM ^2H-Tris-HCl buffer, 100 mM NaCl, 1 mM dithiothreitol (DTT), 0.02% (w/v) NaN_3, 0.05 mM $ZnCl_2$, and 1 mM iminodiacetic acid (IDA), with the addition of D_2O to 10% v/v (pH 7.0). The engineered protein sample used for the NMR measurements comprised 62 amino acid residues and the first 7 residues of the tags. The zf-CW mutants were made using a QuikChange Mutagenesis Kit, and the appropriate mutations were confirmed by DNA sequencing and mass spectrometric analysis. Nonlabeled, synthetic, lyophilized histone tail peptides were purchased from Dharmacon.

NMR Spectroscopy and Resonance Assignments

NMR experiments were performed at 25°C on 600 and 800 MHz spectrometers (Bruker DRX600 and AV800) equipped with *xyz*-pulsed field gradients. Backbone and side-chain assignments were obtained by standard triple resonance experiments (Clore and Gronenborn, 1994). 2D $[^1H,^{15}N]$-HSQC, and 3D HNCO, HN(CA)CO, HNCA, HN(CO)CA, HNCACB, and CBCA(CO)NH spectra were used for the ^1H, ^{15}N, and ^{13}C assignments of the protein backbone. Side-chain ^1H and ^{13}C assignments were obtained using 2D $[^1H,^{13}C]$-HSQC, and 3D HBHA(CO)NH, H(CCCO)NH, (H)CC(CO)NH, HCCH-COSY, HCCH-TOCSY, and (H)CCH-TOCSY spectra. All the assignments were checked for consistency with 3D ^{15}N- and ^{13}C-edited HSQC-NOESY spectra. 3D NOESY spectra were recorded with mixing times of 80 ms. For the assignments of the $H3_{(1-10)}K4me3$ peptide complexed with the zf-CW domain, 2D filtered NOESY spectra with mixing times of 80 and 150 ms, and 2D filtered TOCSY spectra were used (Peterson et al., 2004).

The NMR data were processed with the program NMRPipe (Delaglio et al., 1995). Spectra were analyzed with the programs NMRView (Johnson and Blevins, 1994), KUJIRA (Kobayashi et al., 2007), and SPARKY (T. D. Goddard and D. G. Kneller, SPARKY 3, University of California, San Francisco).

Structure Calculations

Peak lists for the NOESY spectra were generated by interactive peak picking, and peak intensities were determined by the automatic integration function of NMRView (Johnson and Blevins, 1994). The three-dimensional structure was determined by the combined automated NOESY cross-peak assignment and structure calculation with torsion angle dynamics implemented in the CYANA program (Güntert et al., 1997). Restraints for the backbone torsion angles ϕ and φ were determined by a chemical shift database analysis with the program TALOS (Cornilescu et al., 1999). The standard CYANA protocol was applied (Güntert, 2004). In the final refinement stage, distance restraints were added for Zn-S^γ (2.25–2.35 Å) (Summers et al., 1992; Wang et al., 2003) and for the distances between the four zinc-coordinating S^γ atoms, to ensure a tetrahedral zinc coordination geometry. In addition, several hydrogen bonds derived from the NOE network for the β sheet were added for structure refinement. The 20 structures from the CYANA calculation were subjected to restrained energy-refinement with the program AMBER9 (http://amber.scripps.edu) (Case et al., 2005), using the Generalized Born model. During the AMBER calculations, distance and dihedral angle restraints were applied with force constants of 32 kcal mol^{-1} Å^{-1} and 250 kcal mol^{-1} rad^{-2}, respectively. The tetrahedral zinc coordination was restrained by lower and upper distance limits with force constants of 500 kcal mol^{-1} Å^{-1}. PROCHECK_NMR (Laskowski et al., 1996) was used to validate the final structures. Structure figures were prepared with the program MOLMOL (Koradi et al., 1996).

For the determination of the three-dimensional structures of the zf-CW domain-$H3_{(1-10)}K4me3$ complex, the $H3_{(1-10)}K4me3$ resonances were first assigned using the 2D filtered spectra (Peterson et al., 2004). The NOESY cross-peaks were then identified in the 3D ^{15}N- and ^{13}C-HSQC-NOESY spectra of the labeled zf-CW domain with unlabeled $H3_{(1-10)}K4me3$. The intermolecular protein-peptide NOEs were assigned automatically and inspected manually, using the 3D NOESY spectra of the zf-CW domain and the 2D filtered NOESY spectra with mixing times of 80 and 150 ms. Structure calculations were performed in the same manner as for the free zf-CW domain.

NMR Titration Experiments

For the amide chemical shift titration experiments, several N-terminal 20-residue peptides of histones H3 and H4 with and without methylated Lys residues, $H3_{(1-20)}K4me0$, $H3_{(1-20)}K4me1$, $H3_{(1-20)}K4me2$, $H3_{(1-20)}K4me3$, and $H4_{(1-20)}K20me3$, were dissolved in 20 mM *d*-Tris-HCl buffer (pH 7.0),

containing 100 mM NaCl and 1mM *d*-DTT, to make a 5 mM solution. 2D [^{1}H,^{15}N]- and [^{1}H,^{13}C]-HSQC spectra were recorded while increasing the concentration of the peptide relative to that of the zf-CW domain (0.1 mM), to a final 1:3 ratio of zf-CW domain to peptide.

Measurements of Dynamic Parameters

The measurements of the nitrogen relaxation times, T_1 and T_2, and the proton-nitrogen heteronuclear NOEs were performed on a 600 MHz spectrometer with a cryo-probe (Bruker AV 600) at 25°C, using the ^{15}N,^{13}C-labeled zf-CW domain at a concentration of 0.53 mM. Relaxation delays of 5, 65, 145, 246, 366, 527, 757, and 1148 ms were recorded for the measurement of ^{15}N T_1, and relaxation delays of 32, 48, 64, 80, 96, 112, 128, and 144 ms were recorded for the measurement of ^{15}N T_2. The ^{15}N T_1 and ^{15}N T_2 values were extracted using a curve-fitting subroutine included in the program Sparky (T. D. Goddard and D. G. Kneller, SPARKY 3, University of California, San Francisco). The proton-nitrogen heteronuclear NOE values were calculated as the ratio between the cross-peak intensities with and without ^{1}H saturation during relaxation delays. The errors were estimated from the rms value of the baseline noise in the two spectra (Farrow et al., 1994).

ITC Measurements

ITC measurements were performed at 25°C by using a Microcal (Amherst, MA) VP-ITC calorimeter. Samples were buffered with 20 mM Tris-HCl (pH 7.0) and 100 mM NaCl, and were thoroughly degassed before use. First, a 2.0 ml aliquot of about 50 μM zf-CW domain was placed in the cell chamber. The five different solutions for the 10-residue histone H3 peptides (H3$_{(1-10)}$K4me0, H3$_{(1-10)}$K4me1, H3$_{(1-10)}$K4me2, H3$_{(1-10)}$K4me3, and H3$_{(1-11)}$K9me3), at a 20-fold higher concentration, were then injected into it. The heat generated due to dilution of the titrants was very small and was used as a reference for the analysis. The data were analyzed with the Microcal ORIGIN software, using a binding model that assumes a single site of interaction.

ACCESSION NUMBERS

The 20 energy-refined conformers of the ZCWPW1 zf-CW domain (residues 246–307), free and in complex with residues 1–10 of the histone H3 trimethylated at K4, have been deposited in the Protein Data Bank (PDB entries 2E61 and 2RR4, respectively). The chemical shift assignments have been deposited in the BioMagResBank database, with the accession code 11115.

SUPPLEMENTAL INFORMATION

Supplemental Information includes four figures and can be found with this article online at doi:10.1016/j.str.2010.06.012.

REFERENCES

Adams-Cioaba, M.A., and Min, J. (2009). Structure and function of histone methylation binding proteins. Biochem. Cell Biol. *87*, 93–105.

Case, D.A., Cheatham, T.E., 3rd, Darden, T., Gohlke, H., Luo, R., Merz, K.M., Jr., Onufriev, A., Simmerling, C., Wang, B., and Woods, R.J. (2005). The Amber biomolecular simulation programs. J. Comput. Chem. *26*, 1668–1688.

Ciccone, D.N., Su, H., Hevi, S., Gay, F., Lei, H., Bajko, J., Xu, G., Li, E., and Chen, T. (2009). KDM1B is a histone H3K4 demethylase required to establish maternal genomic imprints. Nature *461*, 415–418.

Clore, G.M., and Gronenborn, A.M. (1994). Multidimensional heteronuclear nuclear magnetic resonance of proteins. Methods Enzymol. *239*, 349–363.

Cornilescu, G., Delaglio, F., and Bax, A. (1999). Protein backbone angle restraints from searching a database for chemical shift and sequence homology. J. Biomol. NMR *13*, 289–302.

Delaglio, F., Grzesiek, S., Vuister, G.W., Zhu, G., Pfeifer, J., and Bax, A. (1995). NMRPipe: a multidimensional spectral processing system based on UNIX pipes. J. Biomol. NMR *6*, 277–293.

Farrow, N.A., Muhandiram, R., Singer, A.U., Pascal, S.M., Kay, C.M., Gish, G., Shoelson, S.E., Pawson, T., Forman-Kay, J.D., and Kay, L.E. (1994). Backbone dynamics of a free and phosphopeptide-complexed Src homology 2 domain studied by ^{15}N NMR relaxation. Biochemistry *33*, 5984–6003.

Flanagan, J.F., Mi, L.Z., Chruszcz, M., Cymborowski, M., Clines, K.L., Kim, Y., Minor, W., Rastinejad, F., and Khorasanizadeh, S. (2005). Double chromodomains cooperate to recognize the methylated histone H3 tail. Nature *438*, 1181–1185.

Grini, P.E., Thorstensen, T., Alm, V., Vizcay-Barrena, G., Windju, S.S., Jorstad, T.S., Wilson, Z.A., and Aalen, R.B. (2009). The ASH1 HOMOLOG 2 (ASHH2) histone H3 methyltransferase is required for ovule and anther development in Arabidopsis. PLoS ONE *4*, e7817. doi: 10.1371/journal.pone.0007817.

Güntert, P. (2004). Automated NMR structure calculation with CYANA. Methods Mol. Biol. *278*, 353–378.

Güntert, P., Mumenthaler, C., and Wüthrich, K. (1997). Torsion angle dynamics for NMR structure calculation with the new program DYANA. J. Mol. Biol. *273*, 283–298.

Huang, Y., Fang, J., Bedford, M.T., Zhang, Y., and Xu, R.M. (2006). Recognition of histone H3 lysine-4 methylation by the double tudor domain of JMJD2A. Science *312*, 748–751.

Iyer, L.M., Abhiman, S., and Aravind, L. (2008). MutL homologs in restriction-modification systems and the origin of eukaryotic MORC ATPases. Biol. Direct *3*, 8. doi: 10.1186/1745-6150-3-8.

Johnson, B.A., and Blevins, R.A. (1994). NMR View: A computer program for the visualization and analysis of NMR data. J. Biomol. NMR *4*, 603–614.

Karytinos, A., Forneris, F., Profumo, A., Ciossani, G., Battaglioli, E., Binda, C., and Mattevi, A. (2009). A novel mammalian flavin-dependent histone demethylase. J. Biol. Chem. *284*, 17775–17782.

Kigawa, T., Yabuki, T., Matsuda, N., Matsuda, T., Nakajima, R., Tanaka, A., and Yokoyama, S. (2004). Preparation of Escherichia coli cell extract for highly productive cell-free protein expression. J. Struct. Funct. Genomics *5*, 63–68.

Kim, J., Daniel, J., Espejo, A., Lake, A., Krishna, M., Xia, L., Zhang, Y., and Bedford, M.T. (2006). Tudor, MBT and chromo domains gauge the degree of lysine methylation. EMBO Rep. *7*, 397–403.

Kobayashi, N., Iwahara, J., Koshiba, S., Tomizawa, T., Tochio, N., Güntert, P., Kigawa, T., and Yokoyama, S. (2007). KUJIRA, a package of integrated modules for systematic and interactive analysis of NMR data directed to high-throughput NMR structure studies. J. Biomol. NMR *39*, 31–52.

Koradi, R., Billeter, M., and Wüthrich, K. (1996). MOLMOL: a program for display and analysis of macromolecular structures. J. Mol. Graph. *14*, 51-55, 29-32.

Lan, F., Collins, R.E., De Cegli, R., Alpatov, R., Horton, J.R., Shi, X., Gozani, O., Cheng, X., and Shi, Y. (2007). Recognition of unmethylated histone H3 lysine 4 links BHC80 to LSD1-mediated gene repression. Nature *448*, 718–722.

Laskowski, R.A., Rullmann, J.A., MacArthur, M.W., Kaptein, R., and Thornton, J.M. (1996). AQUA and PROCHECK-NMR: programs for checking the quality of protein structures solved by NMR. J. Biomol. NMR *8*, 477–486.

Lee, M.S., Palmer, A.G., 3rd, and Wright, P.E. (1992). Relationship between ^{1}H and ^{13}C NMR chemical shifts and the secondary and tertiary structure of a zinc finger peptide. J. Biomol. NMR *2*, 307–322.

Li, H., Ilin, S., Wang, W., Duncan, E.M., Wysocka, J., Allis, C.D., and Patel, D.J. (2006). Molecular basis for site-specific read-out of histone H3K4me3 by the BPTF PHD finger of NURF. Nature *442*, 91–95.

Li, H., Fischle, W., Wang, W., Duncan, E.M., Liang, L., Murakami-Ishibe, S., Allis, C.D., and Patel, D.J. (2007). Structural basis for lower lysine methylation state-specific readout by MBT repeats of L3MBTL1 and an engineered PHD finger. Mol. Cell *28*, 677–691.

Matsuda, T., Kigawa, T., Koshiba, S., Inoue, M., Aoki, M., Yamasaki, K., Seki, M., Shinozaki, K., and Yokoyama, S. (2006). Cell-free synthesis of zinc-binding proteins. J. Struct. Funct. Genomics *7*, 93–100.

Pena, P.V., Davrazou, F., Shi, X., Walter, K.L., Verkhusha, V.V., Gozani, O., Zhao, R., and Kutateladze, T.G. (2006). Molecular mechanism of histone H3K4me3 recognition by plant homeodomain of ING2. Nature *442*, 100–103.

Perry, J., and Zhao, Y. (2003). The CW domain, a structural module shared amongst vertebrates, vertebrate-infecting parasites and higher plants. Trends Biochem. Sci. *28*, 576–580.

Peterson, R.D., Theimer, C.A., Wu, H., and Feigon, J. (2004). New applications of 2D filtered/edited NOESY for assignment and structure elucidation of RNA and RNA-protein complexes. J. Biomol. NMR *28*, 59–67.

Shi, Y., Lan, F., Matson, C., Mulligan, P., Whetstine, J.R., Cole, P.A., Casero, R.A., and Shi, Y. (2004). Histone demethylation mediated by the nuclear amine oxidase homolog LSD1. Cell *119*, 941–953.

Summers, M.F., Henderson, L.E., Chance, M.R., South, T.L., Blake, P.R., Perez-Alvarado, G., Bess, J.W., Jr., Sowder, R.C., 3rd, Arthur, L.O., Sagi, I.,

and Hare, D.R. (1992). Nucleocapsid zinc fingers detected in retroviruses: EXAFS studies of intact viruses and the solution-state structure of the nucleocapsid protein from HIV-1. Protein Sci. *1*, 563–574.

Taverna, S.D., Li, H., Ruthenburg, A.J., Allis, C.D., and Patel, D.J. (2007). How chromatin-binding modules interpret histone modifications: lessons from professional pocket pickers. Nat. Struct. Mol. Biol. *14*, 1025–1040.

Wang, B., Alam, S.L., Meyer, H.H., Payne, M., Stemmler, T.L., Davis, D.R., and Sundquist, W.I. (2003). Structure and ubiquitin interactions of the conserved zinc finger domain of Npl4. J. Biol. Chem. *278*, 20225–20234.

Wang, G.G., Song, J., Wang, Z., Dormann, H.L., Casadio, F., Li, H., Luo, J.L., Patel, D.J., and Allis, C.D. (2009a). Haematopoietic malignancies caused by dysregulation of a chromatin-binding PHD finger. Nature *459*, 847–851.

Wang, Y., Reddy, B., Thompson, J., Wang, H., Noma, K., Yates, J.R., 3rd, and Jia, S. (2009b). Regulation of Set9-mediated H4K20 methylation by a PWWP domain protein. Mol. Cell *33*, 428–437.

Xu, L., Zhao, Z., Dong, A., Soubigou-Taconnat, L., Renou, J.P., Steinmetz, A., and Shen, W.H. (2008). Di- and tri- but not monomethylation on histone H3 lysine 36 marks active transcription of genes involved in flowering time regulation and other processes in Arabidopsis thaliana. Mol. Cel Biol. *28*, 1348–1360.

Zhao, Z., Yu, Y., Meyer, D., Wu, C., and Shen, W.H. (2005). Prevention of early flowering by expression of FLOWERING LOCUS C requires methylation of histone H3 K36. Nat. Cell Biol. *7*, 1256–1260.